32nd URSI GASS, Montreal, 19–26 August 2017

Characterization of Indoor Massive MIMO Channel at 11 GHz

Jianzhi Li(1), Bo Ai*(1)(2), Ruisi He(1), Mi Yang(1), Yu Zhang(1), Xin Liu(1), and Zhangdui Zhong(1)
(1) State Key Laboratory of Rail Traffic Control and Safety, Beijing Jiaotong University, Beijing, China
(2) Engineering University of Armed Police Force, Dept. Telecommunication Engineering, Shaanxi, Xi'an, 710086, China
Bo Ai* (Corresponding Author). e-mail: boai@bjtu.edu.cn

Abstract

In this paper, we present a measurement campaign of indoor massive MIMO channels by using a wideband channel sounder and a rectangular large-scale array with 256 elements. The measurements are conducted at 11 GHz, with a bandwidth of 200 MHz, and the light-of-sight (LOS) scenario is considered. Some basic channel parameters, including shadow fading, delay spread and coherence bandwidth, are extracted. The non-stationarity of radio channels, which is reflected by the variations of delay spread and coherence bandwidth over different array locations, is discussed. The results would be useful for the channel modeling of massive MIMO at the frequency bands beyond 6 GHz in the indoor environments.

1 Introduction

The researches on the fifth generation mobile communication system (5G) have been extensively carried out [1], and massive MIMO, which is one of the most important technique of 5G [2–4], has gained more and more attention by researchers. However, in channel modeling of massive MIMO, only few researches and channel measurements are reported [5–7]. The management of spectrum use for 5G is still a debatable issue, however it is reasonble to believe that in order to achieve the best spectrum utilization, the massive MIMO systems working at the frequency bands below 6 GHz are expected to support a large coverage and provide the basic user experience rate, whereas the systems working at the frequency bands beyond 6 GHz are expected to serve for short range communication and carry out wide-bandwidth and high-speed transmissions. Since the system performance can be seriously affected by radio channels, deep investigations on channel behaviors in different typical scenarios (e.g. office, library, railway station, and high-speed railway [8,9], etc) at different frequency bands are required. In this paper, we perform a measurement campaign in a theater environment at 11 GHz, and channel characterization is presented, which is used to give insights to channel modeling of massive MIMO at a the frequency beyond 6 GHz.

The rest of the paper is organized as follows. Section 2 describes the measurement system and measurement environment. Section 3 presents the measurement results and statistical analysis results and Section 4 gives the conclusions of the paper.

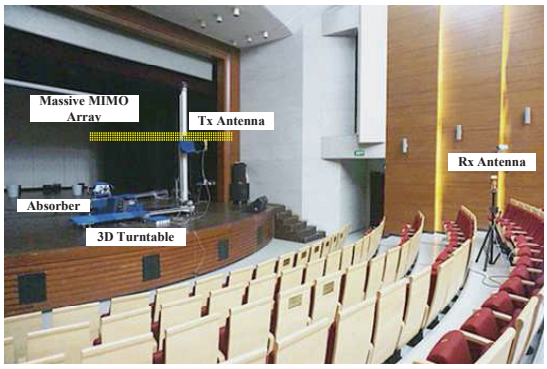

Figure 1. Measurement environment. The elements of the vitual Tx array (4×64) are marked with yellow dots.

2 Measurement Campaign

2.1 Measurement System

The measurement is conducted with a wideband frequency domain channel sounder at 11 GHz. A 256-element virtual rectangular array (URA), which has 64 elements in each rows and 4 elements in each column, is used. The omnidirectional vertical-polarization transmitter (Tx) antenna is moved along the guide rail of the turntable to constitute a 256-element virtual array during the measurements. The 3D turntable can guarantee a millimeter grade of accuracy. Full automatic control of the 3D turntable is realized, which means that the route of the Tx antenna has been preset through programming. An omnidirectional vertical polarization antenna is positioned at 2 points, which are spaced by half a wavelength at each Rx location. The spacing of adjacent antenna elements for Tx is also half a wavelength. The measurement bandwidth 200 MHz, which guarantees a high resolution capability of multipath in the delay domain. The calibration measurements were performed in a anechoic chamber, in order to remove the influence of the sounder equipments, cables and power amplifier. All clocks

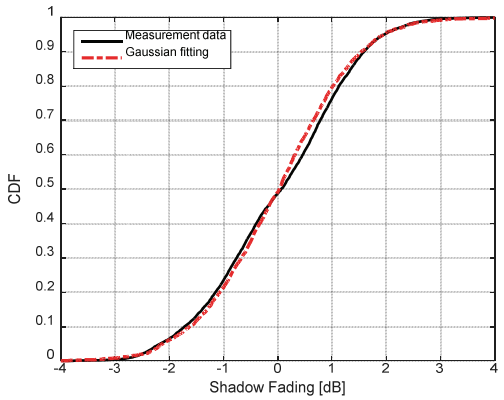

Figure 2. CDF of Shadow Fading with Gaussian fitting.

and sampling circuits in both the Tx and the Rx equipments were slaved to the calibrated rubidium clock at the Tx side, which is disciplined by the Global Positioning System (GPS) before the measurements.

2.2 Measurement Environment

The measurement campaign is conducted at a theater in Student Activity Center, Beijing Jiaotong University, China, as shown in Fig 1. The auditorium of the theater is 15.97 m of length, 11.74 m of width, and 6.92 m of height. In the measurements, the theater is closed and there is no movement of people in order to keep the channel strictly static. The 3D turntable is placed on the left, anterior side of the platform, which is 1.23 m above the ground of theater. The height of Tx antenna is 2.0 m, hence it is 3.23 m above the ground of the theater. During our measurements, the location of the Tx array is fixed, and 18 locations of the Rx are predefined among the auditorium. The distance between Tx and Rx ranges from 5.48 m to 14.27 m.

3 Analysis and Results

The IQ data, which can be used to determine the channel transfer function $H(f)$, is recorded in the frequency domain vector signal analyzer at Rx system during the measurements. The channel impulse response (CIR), $h(\tau)$, can be caculated from the transfer function as

$$h(\tau) = \mathrm{IFFT}(H(f), N_f), \tag{1}$$

where $\mathrm{IFFT}(\cdot)$ is the inverse discrete Fourier transform, τ is delay, and $N_f = 513$ is the number of measured frequency points. A Hann window is used to suppress side lobes.

3.1 Path loss and Shadow Fading

The local wideband path loss is determined from the measured transfer functions. The dB-scale path loss can be caculated as follow [10]

$$\mathrm{PL} = -10\log_{10}\left(\frac{1}{N_f}\sum_{l=1}^{N_f}|H(f_l)|^2\right), \tag{2}$$

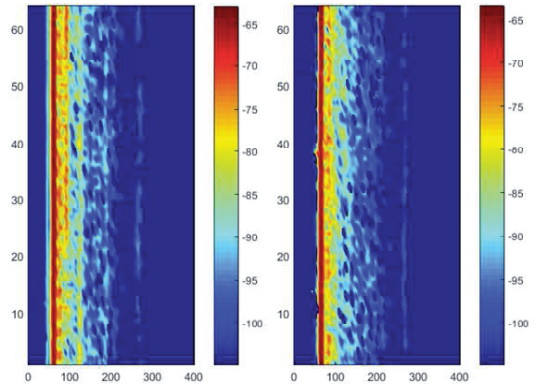

Figure 3. Example plot of PDPs along the 4-th row of the URA. (a) Row NO.6, Seat NO.7. (b) Row NO.8, Seat NO.2.

where f_l is the l-th frequency point in the measured transfer function. In our measurements, since the range from Tx to Rx is short, we focus on the shadow fading. The dB-scale shadow fading can be conventionally modeled as a real zero-mean Gaussian process with a standard deviation of σ_S as [11–13]

$$X_S \sim N\left(0, {\sigma_S}^2\right). \tag{3}$$

Fig. 2 shows the esitmated cumulative distribution function (CDF) of shadow fading with a Gaussian fit. The corresponding σ_S is found to be 1.27 dB. In [14], a measurement campaign of MIMO channels in conducted at 11 GHz in the indoor environments. Our result is similar to the result therein, which is useful to channel modeling of massive MIMO in indoor scenarios.

3.2 Power Delay Profile and RMS Delay Spread

RMS Delay Spread is a typical parameter to depicts the channel temporal dispersion, which can be caculated from the average power delay profile (APDP). APDP can be obtained from the CIR, as follow [11, 15]

$$\mathrm{APDP}(\tau) = \frac{1}{N_{cyc}}\sum_{i=1}^{N_{cyc}}\mathrm{PDP}(\tau, t_i) = \frac{1}{N_{cyc}}\sum_{i=1}^{N_{cyc}}|h(\tau, t_i)|^2, \tag{4}$$

where $N_{cyc} = 12$ is the number of the PDP samples in each sunchannels. t_i is the i-th time instant. Fig. 3 shows example plots of the measured APDPs for the 256-element URA. In order to perform a quantitative analysis, we set a noise threshold to eliminate the impact of noise, and calculate the root-mean-square (RMS) delay spread. The noise threshold is set to be 6 dB above the noise floor [16]. RMS delay spread can be obtained by [11]

$$\tau_{\mathrm{rms}} = \sqrt{\frac{\sum_p \mathrm{APDP}(\tau_p)\tau_p^2}{\sum_p \mathrm{APDP}(\tau_p)} - \left(\frac{\sum_p \mathrm{APDP}(\tau_p)\tau_p}{\sum_p \mathrm{APDP}(\tau_p)}\right)^2}, \tag{5}$$

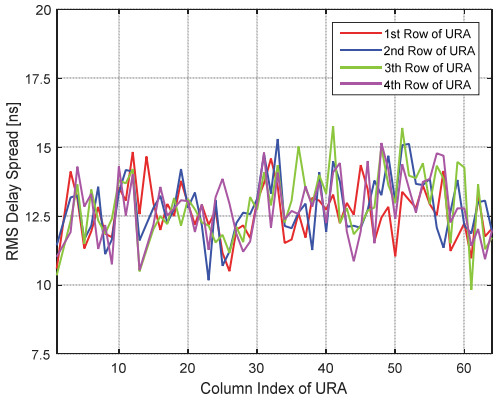

Figure 4. Estimated RMS delay spread for the Rx location of Row NO.8 & Seat NO.2.

where τ_p denotes the p-th delay bin of the corresponding APDP. Fig. 4 illustrates an example plot of the estimated RMS delay spread for the Rx location of Row NO.8 & Seat NO.2. The RMS delay spreads for all the 18 Rx locations are estimated, the mean and standard deviation are found to be 14.17 ns and 2.30 ns, respectively. These results are relatively smaller compared with [14], probably due to the different propagation environment and data processing method. Moreover, we compare these results with the ones in [7], which performs a measurement campaign of massive MIMO channels at the frequency bands below 6 GHz in an indoor lecture hall. The means of RMS delay spread in [7] are generally larger than 25 ns, which is relatively larger than the result in this paper. However, the standard deviations of RMS delay spread are 2.1∼2.8 ns overall, which is fairly close to the result of 11 GHz. It is found that, in an indoor environment with a carrier frequency of 11 GHz, the channel characteristics of massive MIMO are non-stationary in both spatial and delay domains.

3.3 Coherence Bandwidth

We use coherence bandwidth B_{coh} to characterise the channel behavior in the frequency domain. It defines the smallest bandwidth of which the correlation between fading at two different frequencies is under a given threshold (e.g $1/e$). The frequency correlation function (FCF), R_H, can be obtained as [11]

$$R_H(\Delta f) = \text{FFT}\left(\text{APDP}\left(\tau\right), N_\tau\right), \tag{6}$$

where $\text{FFT}\left(\cdot\right)$ denotes the fourier transform and N_τ is the numbers of delay bins. Once the correlation function is obtained, the coherence bandwidth can be determined in terms of a correlation level of $1/e$. Fig. 5 illustrates the FCFs at the Rx location of Row NO.8 & Seat NO.2. The corresponding coherence bandwidth is shown in Fig. 6. The coherence bandwidths of all 18 Rx locations are estimated, the mean and standard deviation are found to be 66.94 MHz and 8.62 MHz, respectively. It is noticed that the coherence bandwidth varies along the Tx array.

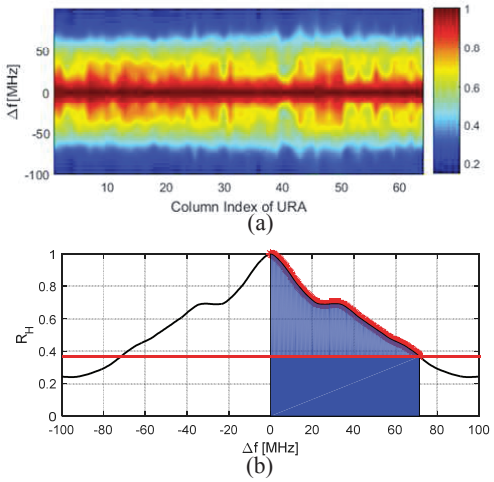

Figure 5. Example plots of correlation functions for the Rx location of Row NO.8 & Seat NO.2. (a) Correlation functions along the 3-th rows of URA. (b) Correlation function corresponding to the 32-th subchannel along the 3-th rows of URA, together with the threshold of $1/e$.

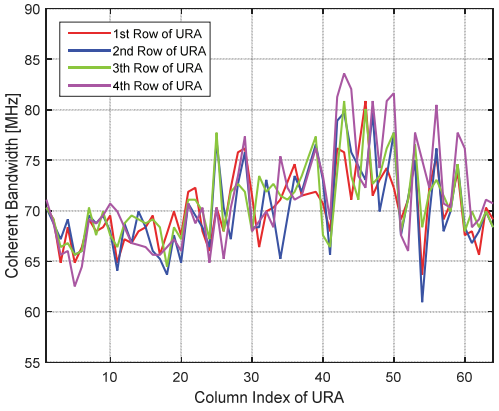

Figure 6. Estimated coherence bandwidth for the Rx location of Row NO.8 & Seat NO.2.

4 Conlusion

A measurement campaign of massive MIMO channels was carried out in an indoor theater environment at 11 GHz with a bandwidth of 200 MHz. A 256-element URA (4×64) was used at the Tx side, and 18 different Rx locations among the auditorium were used in the measurements. Some typical channel parameters are extracted and analysized, such as shadow fading, RMS delay spread and coherence bandwidth. The standard deviation of shadowing is 1.27 dB. The means and the standard deviation of RMS delay spread are 14.17 ns and 2.30 ns, and the means and the standard deviation of coherence bandwiddth are found to be 66.94 MHz and 8.62 MHz, respectively. It is found that the non-stationarity of the massive MIMO channel also exists at 11 GHz band, and this feature should be handled carefully when modeling massive MIMO channels.

5 Acknowledgements

Project supported by the National Natural Science Foundation of China under Grant 61501020, the State Key Laboratory of Rail Traffic Control and Safety under Grant RCS2016ZJ005, the National key research and development program under Grant 2016YFB1200102-04, the China Postdoctoral Science Foundation under Grant 2016M591355, the Fundamental Research Funds for the Central Universities (No. 2016JBZ006), the Natural Science Base Research Plan in Shanxi Province of China under Grant 2015JM6320 and the Key Project from Beijing science and Technology Commission under Grant D151100000115004.

References

[1] J. G. Andrews, S. Buzzi, W. Choi, S. V. Hanly, A. Lozano, A. C. K. Soong, and J. C. Zhang, "What will 5g be?," *IEEE Journal on Selected Areas in Communications*, vol. 32, pp. 1065–1082, June 2014.

[2] E. G. Larsson, O. Edfors, F. Tufvesson, and T. L. Marzetta, "Massive mimo for next generation wireless systems," *IEEE Communications Magazine*, vol. 52, pp. 186–195, February 2014.

[3] F. Boccardi, R. W. Heath, A. Lozano, T. L. Marzetta, and P. Popovski, "Five disruptive technology directions for 5g," *IEEE Communications Magazine*, vol. 52, pp. 74–80, February 2014.

[4] Y. Cai, R. C. de Lamare, B. Champagne, B. Qin, and M. Zhao, "Adaptive reduced-rank receive processing based on minimum symbol-error-rate criterion for large-scale multiple-antenna systems," *IEEE Transactions on Communications*, vol. 63, pp. 4185–4201, Nov 2015.

[5] J. Hoydis, C. Hoek, T. Wild, and S. ten Brink, "Channel measurements for large antenna arrays," in *2012 International Symposium on Wireless Communication Systems (ISWCS)*, pp. 811–815, Aug 2012.

[6] X. Gao, O. Edfors, F. Rusek, and F. Tufvesson, "Massive mimo performance evaluation based on measured propagation data," *IEEE Transactions on Wireless Communications*, vol. 14, pp. 3899–3911, July 2015.

[7] J. Li, B. Ai, R. He, K. Guan, Q. Wang, D. Fei, Z. Zhong, Z. Zhao, D. Miao, and H. Guan, "Measurement-based characterizations of indoor massive mimo channels at 2 ghz, 4 ghz, and 6 ghz frequency bands," in *2016 IEEE 83rd Vehicular Technology Conference (VTC Spring)*, pp. 1–5, May 2016.

[8] B. Ai, K. Guan, M. Rupp, T. Kurner, X. Cheng, X. F. Yin, Q. Wang, G. Y. Ma, Y. Li, L. Xiong, and J. W. Ding, "Future railway services-oriented mobile communications network," *IEEE Communications Magazine*, vol. 53, pp. 78–85, October 2015.

[9] B. Ai, X. Cheng, T. Kürner, Z. D. Zhong, K. Guan, R. S. He, L. Xiong, D. W. Matolak, D. G. Michelson, and C. Briso-Rodriguez, "Challenges toward wireless communications for high-speed railway," *IEEE Transactions on Intelligent Transportation Systems*, vol. 15, pp. 2143–2158, Oct 2014.

[10] R. He, A. F. Molisch, F. Tufvesson, Z. Zhong, B. Ai, and T. Zhang, "Vehicle-to-vehicle propagation models with large vehicle obstructions," *IEEE Transactions on Intelligent Transportation Systems*, vol. 15, pp. 2237–2248, Oct 2014.

[11] A. F. Molisch, *Wireless Communications*. Wiley Publishing, 2nd ed., 2011.

[12] R. He, Z. Zhong, B. Ai, G. Wang, J. Ding, and A. F. Molisch, "Measurements and analysis of propagation channels in high-speed railway viaducts," *IEEE Transactions on Wireless Communications*, vol. 12, pp. 794–805, February 2013.

[13] R. He, Z. Zhong, B. Ai, and J. Ding, "An empirical path loss model and fading analysis for high-speed railway viaduct scenarios," *IEEE Antennas and Wireless Propagation Letters*, vol. 10, pp. 808–812, 2011.

[14] M. Kim, Y. Konishi, Y. Chang, and J. i. Takada, "Large scale parameters and double-directional characterization of indoor wideband radio multipath channels at 11 ghz," *IEEE Transactions on Antennas and Propagation*, vol. 62, pp. 430–441, Jan 2014.

[15] R. He, W. Chen, B. Ai, A. F. Molisch, W. Wang, Z. Zhong, J. Yu, and S. Sangodoyin, "On the clustering of radio channel impulse responses using sparsity-based methods," *IEEE Transactions on Antennas and Propagation*, vol. 64, pp. 2465–2474, June 2016.

[16] A. F. Molisch and M. Steinbauer, "Condensed parameters for characterizing wideband mobile radio channels," *International Journal of Wireless Information Networks*, vol. 6, no. 3, pp. 133–154, 1999.